

New Transparent Laser-Drilled Fluorine-doped Tin Oxide covered Quartz Electrodes for Photo-Electrochemical Water Splitting

Original

New Transparent Laser-Drilled Fluorine-doped Tin Oxide covered Quartz Electrodes for Photo-Electrochemical Water Splitting / HERNANDEZ RIBULLEN, SIMELYS PRIS; Tortello, Mauro; Sacco, Adriano; Quaglio, Marzia; Toby, Meyer; Bianco, Stefano; Saracco, Guido; Pirri, Candido; Tresso, Elena Maria. - In: ELECTROCHIMICA ACTA. - ISSN 0013-4686. - 131:(2014), pp. 184-194. [10.1016/j.electacta.2014.01.037]

Availability:

This version is available at: 11583/2588509 since: 2016-08-25T18:45:18Z

Publisher:

ELSEVIER

Published

DOI:10.1016/j.electacta.2014.01.037

Terms of use:

This article is made available under terms and conditions as specified in the corresponding bibliographic description in the repository

Publisher copyright

(Article begins on next page)

Citation Information:

Simelys Hernández, Mauro Tortello, Adriano Sacco, Marzia Quaglio, Toby Meyer, Stefano Bianco, Guido Saracco, C. Fabrizio Pirri, Elena Tresso

New Transparent Laser-Drilled Fluorine-doped Tin Oxide covered Quartz Electrodes for Photo-Electrochemical Water Splitting,

Electrochimica Acta, 131 (2014) 184–194, DOI: <http://dx.doi.org/10.1016/j.electacta.2014.01.037>.

Electrochimica Acta 131 (2014) 184–194



Contents lists available at ScienceDirect

Electrochimica Acta

journal homepage: www.elsevier.com/locate/electacta



New Transparent Laser-Drilled Fluorine-doped Tin Oxide covered Quartz Electrodes for Photo-Electrochemical Water Splitting



Simelys Hernández^{a,*}, Mauro Tortello^b, Adriano Sacco^a, Marzia Quaglio^a, Toby Meyer^c, Stefano Bianco^a, Guido Saracco^b, C. Fabrizio Pirri^{a,b}, Elena Tresso^{a,b}

^a Center for Space Human Robotics, IIT@POLITO, Istituto Italiano di Tecnologia, C.so Trento 21, 10129, Turin, Italy

^b Department of Applied Science and Technology (DISAT), Politecnico di Torino, C.so Duca degli Abruzzi 24, 10129, Turin, Italy

^c Solaronix SA, Rue de l'Ouriette 129, CH-1170, Aubonne VD, Switzerland

ARTICLE INFO

Article history:

Received 12 September 2013

Received in revised form 7 January 2014

Accepted 7 January 2014

Available online 21 January 2014

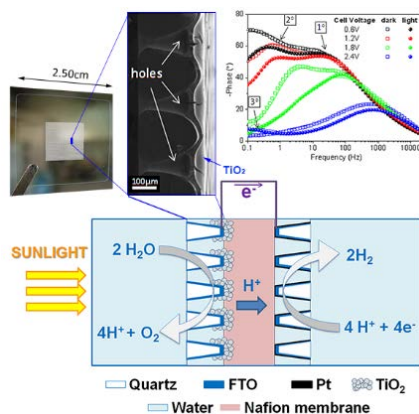
Keywords:

porous electrode
water photo-electrolysis
photo-electrolyzer
electrochemical impedance spectroscopy
FTO

ABSTRACT

A new-designed transparent, conductive and porous electrode was developed for application in a compact laboratory-scale proton exchange membrane (PEM) photo-electrolyzer. The electrode is made of a thin transparent quartz sheet covered with fluorine-doped tin oxide (FTO), in which an array of holes is laser-drilled to allow water and gas permeation. The electrical, morphological, optical and electrochemical characterization of the *drilled* electrodes is presented in comparison with a *non-drilled* one. The drilled electrode exhibits, in the visible region, a good transmittance (average value of 62%), a noticeable reflectance due to the light scattering effect of the hole-drilled internal region, and a higher effective surface area than the non-drilled electrode. The proof-of-concept of the applicability of the drilled electrode was achieved by using it as a support for a traditional photocatalyst (i.e. commercial TiO₂ nanoparticles). The latter, coupled with a polymeric electrolyte membrane (i.e. Nafion 117) and a Pt counter electrode, forms a transparent membrane electrode assembly (MEA), with a good conductivity, wettability and porosity. Electrochemical impedance spectroscopy (EIS) was used as a very powerful tool to gain information on the real active surface of the new *drilled* electrode and the main electrochemical parameters driving the charge transfer reactions on it. This new electrode architecture is demonstrated to be an ideal support for testing new anodic and cathodic photoactive materials working in tandem configuration for solar fuels production by water photo-electrolysis.

© 2014 Elsevier Ltd. All rights reserved.



New Transparent Laser-Drilled Fluorine-doped Tin Oxide covered Quartz Electrodes for Photo-Electrochemical Water Splitting

Simelys Hernández^{1,*}, Mauro Tortello², Adriano Sacco¹, Marzia Quaglio¹, Toby Meyer³, Stefano Bianco¹, Guido Saracco², C. Fabrizio Pirri^{1,2}, Elena Tresso^{1,2}

¹ *Center for Space Human Robotics, IIT@POLITO, Istituto Italiano di Tecnologia, C.so Trento 21, 10129, Turin, Italy.*

² *Department of Applied Science and Technology (DISAT), Politecnico di Torino, C.so Duca degli Abruzzi 24, 10129, Turin, Italy*

³ *Solaronix SA, Rue de l'Ouriette 129, CH-1170, Aubonne VD, Switzerland*

* corresponding author: simelys.hernandez@polito.it, tel. +39.011.0904774

Abstract

A new-designed transparent, conductive and porous electrode was developed for application in a compact laboratory-scale proton exchange membrane (PEM) photo-electrolyzer. The electrode is made of a thin transparent quartz sheet covered with fluorine-doped tin oxide (FTO), in which an array of holes is laser-drilled to allow water and gas permeation. The electrical, morphological, optical and electrochemical characterization of the drilled electrodes is presented in comparison with a non-drilled one. The drilled electrode exhibits, in the visible region, a good transmittance (average value of 62%), a noticeable reflectance due to the light scattering effect of the hole-drilled internal region, and a higher effective surface area than the non-drilled electrode. The proof-of-concept of the applicability of the drilled electrode was achieved by using it as a support for a traditional photocatalyst (i.e. commercial TiO₂ nanoparticles). The latter, coupled with a polymeric electrolyte membrane (i.e. Nafion 117) and a Pt counter electrode, forms a transparent membrane electrode assembly (MEA), with a good conductivity, wettability and porosity. Electrochemical impedance spectroscopy (EIS) was used as a very powerful tool to gain information on the real active surface of the new *drilled* electrode and the main electrochemical parameters driving the charge transfer reactions on it. This new electrode architecture is demonstrated to be an ideal support for testing new anodic and cathodic photoactive materials working in tandem configuration for solar fuels production by water photo-electrolysis.

Keywords: porous electrode, water photo-electrolysis, photo-electrolyzer, electrochemical impedance spectroscopy, FTO

1. Introduction

Also known as “artificial photosynthesis”, the photo-electrochemical water splitting offers a promising way for clean, low-cost, environmentally friendly and virtually inexhaustible fuel production from solar energy. The appealing idea is to use the light from the sun, together with appositely designed semiconducting and catalytic materials, to obtain the water dissociation into elemental hydrogen and oxygen, and eventually the production of hydrocarbon fuels if the generated hydrogen is employed to reduce CO₂. Since 1972, when this concept was firstly developed using a TiO₂ photoelectrode by Fujishima and Honda [1], a lot of efforts have been devoted to obtain materials and devices with the stability, cost and efficiency requirements needed for large-scale applications. On the one hand the research focuses on improving the photocatalyst properties, suggesting nanostructured materials, easy to prepare and highly stable in aqueous solutions and oxygen evolving conditions, generally based on n-type metal oxides [2-6]. On the other hand, the aim is to develop low-cost integrated devices, designing photo-electrochemical cells with high solar power to fuel conversion efficiencies [7-10].

The generally proposed architecture for water splitting devices is based on the presence of separate compartments for the water oxidation and the reduction reactions. The reaction chambers are separated by a proton exchange membrane (PEM), similar to the ones already in use for hydrogen fuel cells (FC) [11, 12] and for water-electrolyzers [13, 14], as proposed in some recent EU-projects [15-17] and by different research groups [7-10, 13-20]. This PEM approach also enables gases generation under pressure, tightening the electrolyzer, which brings about an increased level of safety [21]. Both PEM electrolyzers and PEM photo-electrolyzers are constituted by three principal components [22]: the membrane electrode assembly (MEA) with the anode, the cathode and the polymeric electrolyte membrane (usually made in Nafion [23]); two reaction chambers (respectively anodic and cathodic) where water flows, and the

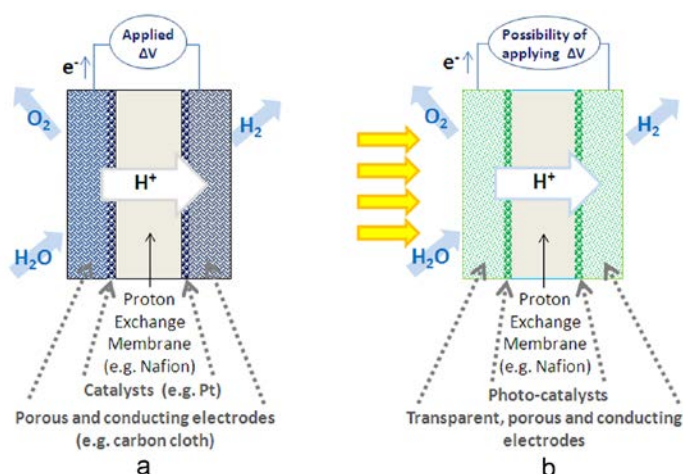


Fig. 1: MEA assemblies for PEM electrolyzer (a) and PEM photo-electrolyzer (b)

housing system, that in PEM photo-electrolyzers has to contain transparent windows for solar light illumination.

The main difference of a PEM photo-electrolyzer with respect to a PEM electrolyzer stands in the MEA, which has to allow the H⁺ transfer to the membrane, the collection of the electrons and the support of the catalysts (see Fig. 1). In PEM electrolyzers, MEAs are generally made in porous and electron conducting materials such as carbon cloth, which is highly conductive, water permeable (so to permit the wetting of the Nafion membrane) and can easily host Pt or other nanoparticle catalysts (see Fig. 1-a) [24, 25]. In PEM photo-electrolyzers, the electrodes have also to support the light harvester material, able to capture the solar photons and to further reduce the bias potential, and the carbon cloth cannot be employed. As shown in Fig. 1-b, the MEA of photo-electrolyzers should be transparent to the light on both the anodic and cathodic side, so that also the cathodic electrode can absorb and take advantage of the part of the solar spectrum not exploited by the anodic material. In PEM electrolyzers the employed MEAs are generally fabricated following the consolidated and well established technology of the gas diffusion electrodes for PEM fuel cells, but in PEM photo-electrolyzers new technological solutions have to be searched. The PEM photo-electrolyzer electrode support has to be electrically conductive (at least on the photocatalyst side), transparent to the visible light, porous, mechanically robust and permit an easy

attachment of catalysts and/or bio-molecules, q-dots, or other photo-active nanoparticles. Despite the fast growing literature on artificial photosynthesis, few papers have till now focused on this subject. Goretex membranes have been employed for “breathable” electrodes providing a good separation of the two gas chambers and decreasing the gas cross-over [26]. Nafion membranes in which photocatalyst (e.g. TiO_2 powder) and Pt powders have been embedded with a suitable amount of conductive carbon black powder [27] have been demonstrated to be a valid alternative when catalysts materials are easily mixable in a Nafion monomer suspension. Also, some novel electrode architectures at the nano- or micro-scopic scale have recently been suggested, even if not yet employed in photo-electrolyzers: 3D-branched nanowires [28], nano-crystalline and macroporous antimony-doped Tin Oxide [29], nano-ITO films with high surface area [30] and free-standing, very thin films of hierarchically porous N-doped graphene [31]. Finally, it has to be observed that, in the impressive number of papers that propose new photocatalytic materials, the characterizations are generally done in electrolytic cells and the materials are generally deposited on a glass substrate, covered by a transparent conductive oxide (TCO) (see for instance: [32-34]). Such transparent electrodes are also used in dye sensitized or thin films solar cells: they are made of glass slides covered with a thin film of a TCO, i.e. ITO (Indium-doped Tin Oxide) or FTO (Fluorine-doped Tin Oxide). However, they cannot be employed in PEM photo-electrolyzers, since they are not porous and hence the gases (O_2 , H_2) produced during the water splitting reaction and the water cannot permeate.

The main aim of this paper is to propose a new design of transparent, conductive and porous electrodes to be employed as support for photo-active materials. These new electrodes offer all the advantages of the TCO/glass substrates: good transparency, low electric resistance and easy adhesion of photocatalysts, moreover they permit the passage of water and gases and can be employed in a MEA assembly for PEM photo-electrolyzers. They have been made with very thin (250 μm) quartz slides in

which an array of holes has been obtained by laser drilling for permitting water and gas flow. An FTO thin film has been deposited on the laser-treated quartz slides to guarantee electrical conductivity. The results of morphological, optical and electrochemical characterization of the electrodes are reported. Moreover, the MEA has been integrated and tested in a simple and easy-to-handle PEM photo-electrolyzer device appositely designed for testing different photo-activated materials. The first water splitting results obtained on laser-drilled FTO/quartz electrodes covered with a traditional photocatalyst (i.e. commercial available TiO_2 nanoparticles) are also presented. Electrochemical impedance spectroscopy (EIS) results, modeled though an equivalent circuit allowing the determination of the electrochemical parameters that can help in the optimization of both the photo-electrode and the device, are finally reported and discussed.

2. EXPERIMENTAL

2.1. Electrodes Preparation

Very thin quartz plates (250 μm -thick, 2.5 x 2.5 cm^2) were laser-drilled and subsequently covered by an FTO layer. By using an electronically pulsed Model L48-1 Synrad CO_2 10 W laser source (driven by a UC-1000 Synrad controller) mounted on a modified Deltatech D700 X-Y table (by Solaronix) an array of 1659 holes was drilled over the central region (1x1 cm^2) of the quartz plates. The holes dimensions and spacing were carefully chosen in order to guarantee robustness, electrical conductivity and permeation to water and gas molecules. The drilled quartz sheets were spin-coated with a thin TiO_2 buffer-film (thickness of about 25 nm) in order to guarantee good adhesion. They were then covered on one side with an FTO layer (thickness of 150 nm), deposited by atmospheric pressure chemical vapor deposition at a temperature of 500 $^\circ\text{C}$. A non-drilled quartz slide was covered with a continuous FTO film with the same procedure and used as a reference for comparison purposes. Below, these two electrodes will be called “drilled” and “non-drilled” respectively.

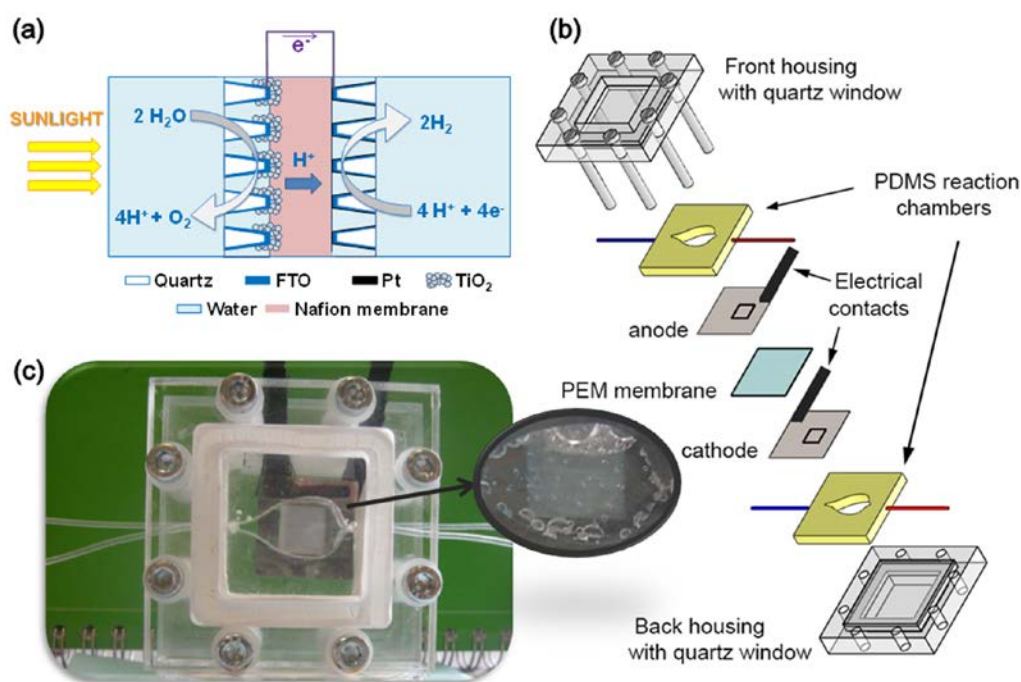


Fig. 2: PEM photo-electrolyzer exploiting drilled electrodes: (a) scheme, (b) exploded view of the assembly design, and (c) photograph of the cell using the TiO_2 /drilled electrode as anode and the Pt/drilled electrode as cathode (inset: view of the anodic chamber with O_2 bubbles formed during the test).

Photo-electrodes were prepared by depositing a thick film of TiO_2 nanoparticles on the FTO-side of drilled electrode. The substrates were firstly cleaned for 3 min in acetone and 3 min in ethanol in an ultrasonic bath and then a titania film was spread by the doctor blade method using a commercial paste (DSL 18NR-T by Dyesol). The film was annealed in a programmable furnace at 450 °C for 30 min in calm Air, using a heating rate of 5 °C/min, and then cooled down naturally. Below, these electrodes will be referred to as “*TiO₂/drilled*”.

Cathodes were fabricated by depositing a thin and dense film of Pt (thickness of about 110 nm) on FTO-drilled electrodes. The drilled substrates were first cleaned with a pre-sputtering procedure in Ar plasma at 20 mA for 5 min and then Pt was deposited by sputtering (Quorum Q150TES) at 30 mA for 320 s. Below, these electrodes will be called “*Pt/drilled*”.

2.2. Electrodes Characterization

An optical microscope (Edmund Scientific binocular fit with a Moticam 1000 camera) and a ZEISS Supra 40 field emission scanning electron microscope (FESEM) were used for morphological

characterizations. UV-Vis diffuse transmittance and reflectance spectra were measured using a Varian-Cary 500 spectrophotometer equipped with an integrating sphere.

Optical contact angle (OCA) measurements were performed with an OCAH 200 instrument (DataPhysic Instruments GmbH), equipped with a charge-coupled device camera and an automatic dosing system for the liquid. Deionized water MilliQ grade (H_2O) was used as the liquid for the analysis (droplet volume=1.5 μl), using the sessile droplet method in static mode. The measurements were performed at ambient conditions on the drilled electrodes, with and without the thick TiO_2 film. Pictures of the drops were collected immediately after the contact with the surface. Drop profiles were fitted through the Young–Laplace method, and contact angles between fitted function and baseline were calculated by the SCA20 software [35].

The electrical conductivity of *drilled* and *non-drilled* electrodes was evaluated with four-point probe measurements using a Keithley 2440 source-measure unit.

2.3. PEM photo-electrolyzer device assembly

An appositely designed PEM photo-electrolyzer has been fabricated to study the photo-electrochemical performance of the *TiO₂/drilled* electrode for the water splitting reaction, as a case study. Fig. 2 shows the scheme of the PEM photo-electrolyzer assembly that uses the *TiO₂/drilled* electrode as anode, the *Pt/drilled* electrode as cathode, and Nafion 117 as proton conducting membrane. These three elements constitutes the MEA which is sandwiched between two microfluidic reaction chambers made of polydimethylsiloxane (PDMS), closed by two quartz windows placed at the front and at the back side of the device, respectively (see Fig.2-b). Both reaction chambers contain a water volume of 1.6 cm³, noticeably lower than the quantity normally used in electrochemical cells. The microfluidic architecture of the reaction chamber permits to optimize the flow of the fluids moving into the device not only by the proper positioning of the inlet and outlet ports, but also thanks to its particular shape. In fact the chamber has a drop-like structure which favors the liquid flow and avoids gas accumulation. PDMS is chemically stable and inert to the reactions occurring into the cell, and moreover its transparency permits optical inspection during tests (see Fig. 2-c). A clamping system made of polycarbonate was used to keep in position the quartz windows, the PDMS chambers and the MEA while applying the pressure necessary to seal the photo-electrolyzer.

Prior to the test, the Nafion 117 membrane was protonated and humidified in an aqueous solution of H₂SO₄ (0.1 M) for 48 hours at room temperature, in order to obtain an optimal and reproducible proton conductivity during the tests, since the focus of the work is on the innovative electrode and not on the membrane itself. It was subsequently sandwiched between the TiO₂ side and the Pt side of the drilled electrodes to minimize the distance between the two-electroactive surfaces. The prepared MEA was closed between the two PDMS chambers and the quartz windows. Two slices of carbon cloth have been used for the electrical contact between the FTO surface and

the external electrical circuit in both electrodes. In Fig. 2-c a photograph of the final assembly is reported. The reaction chambers were filled and fed continuously with an electrolytic solution of Sodium Phosphate Buffer (0.1 M, pH=7.0), using a peristaltic pump (Peripro-4H by Word Precision Instruments) at a rate of 5 ml/min: such value is able to guarantee continuous electrolyte regeneration and exit of produced gases in the reaction chambers.

2.4. Electrochemical and photo-electrochemical characterizations

The *drilled* and the *non-drilled* electrodes have been electrochemically characterized using them as anodes for the water electrolysis reaction. A *Pt/drilled* electrode was used as the cathode. Tests were performed in an electrochemical pyrex glass cell containing 40 cm³ of aqueous solution of sodium phosphate buffer (0.1 M, pH=7.0) at 25 °C as liquid electrolyte. A two-electrodes configuration has been adopted using the anode as working electrode and the *Pt/drilled* as counter electrode, with anode-cathode distance of about 1 cm, facing on the conductive side. The reference electrode of the potentiostat (VSP by BioLogic Science instruments) was short-circuited with the counter electrode. In order to obtain the stationary conditions necessary for impedance measurements, the cell containing the anode under test was first polarized at 3 V for 1 h and then the current-voltage (*I-V*) curve was measured through a linear sweep voltammetry (LSV) at a rate of 20 mV/s from 0 V to 3 V. The EIS curves were recorded in the frequency range of 1 MHz to 100 mHz, with an ac amplitude of 25 mV, every 0.3 V in the range 0-3 V.

In the PEM photo-electrolyzer the electrochemical tests were performed at ambient temperature in two-electrodes configuration, using the *TiO₂/drilled* electrode as anode and working electrode, and the *Pt/*

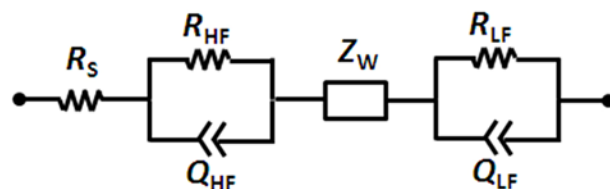


Fig. 3: Equivalent circuit for modeling of EIS data.

drilled as cathode, counter and reference electrode, with the VSP potentiostat. The photo-electrolyzer was first polarized at 2 V for 1 h to allow a full development of the concentration gradients in the cell. Then, the *I-V* characteristic curve was measured by applying an external potential bias between 0 and 2.5 V at a rate of 20 mV/s. EIS curves were then recorded in the frequency range of 1 MHz to 100 mHz with an ac amplitude of 25 mV, every 0.3 V in the range 0-2.5 V. LSV and EIS measurements were performed under dark and under frontal simulated AM 1.5G solar light illumination (100 mW/cm² irradiation, provided by a 450 W Xe lamp with an A.M. 1.5 filter and a water filter), cutting off IR radiation in order to avoid the heating of the device.

In both cases, the reported current densities were calculated using the geometrical area of the anodic electrodes in contact with the liquid electrolyte: 4.38 cm² in the first case and 1.59 cm² in the second one. Moreover, the impedance spectras were fitted by means of the ZSimpWin (EChemSoftware) software, using the equivalent electrical circuit shown in Fig. 3, previously reported in the literature for the study of porous and semiconducting electrodes [3, 10, 36], as well as to represent electrode interfaces (anode and cathode) in fuel cell systems [37].

3. RESULTS and DISCUSSION

3.1. Morphological, electrical and optical properties of the electrodes

A scheme of the transversal view of the *drilled* electrode, a picture of the laser-treated quartz slide and

an optical microscope image of the array of holes are shown in Figs 4-a, b and c, respectively. Moreover, FESEM pictures showing the top view (FTO side) of the *drilled* electrode and a magnified zoom of a single hole are reported in Figs 5-a, b and c, respectively. As it can be observed by Figs 4 and 5, the holes pass through the quartz slide with a truncated conical shape, typical of the laser drilling process, with a high regularity and homogeneity on shape and dimension. The larger side of the cone is about 150 μm at the FTO side and the smaller about 30 μm at the quartz back side; the deposited FTO partially covers also the internal surface of the holes. In this way it is possible to obtain a porous film of transparent conductive oxide characterized by large holes (permitting high wettability of the Nafion membrane) and by high surface area (increasing the available surface for catalyst molecules attachment). Results of the optical measurements in the UV-Vis range are shown in Fig. 6. In the transmittance and reflectance spectra of the *non-drilled* electrodes (Fig. 6-b) the interference fringes due to the FTO uniform thin film are clearly visible. Moreover, as expected, the *non-drilled* electrodes exhibit very high transparency in the visible region, with an average transmittance value equal to 81% for wavelengths between 400 and 700 nm. In the spectra of the *drilled* electrodes (Fig. 6-a) the transparency in the visible range is lower (the average transmittance value is 62%) but a noticeable increase in reflectance is observed, due to the light scattering effect of the hole-drilled internal region of the electrode. For *non-drilled* electrodes the visible average reflectance (only given by the specular

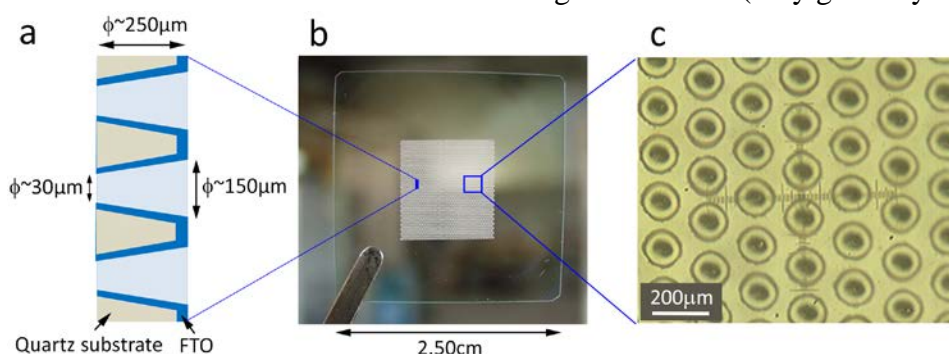


Fig. 4: The laser-drilled electrode: (a) scheme of cross-section, (b) photograph and (c) optical microscopy image (view from FTO side).

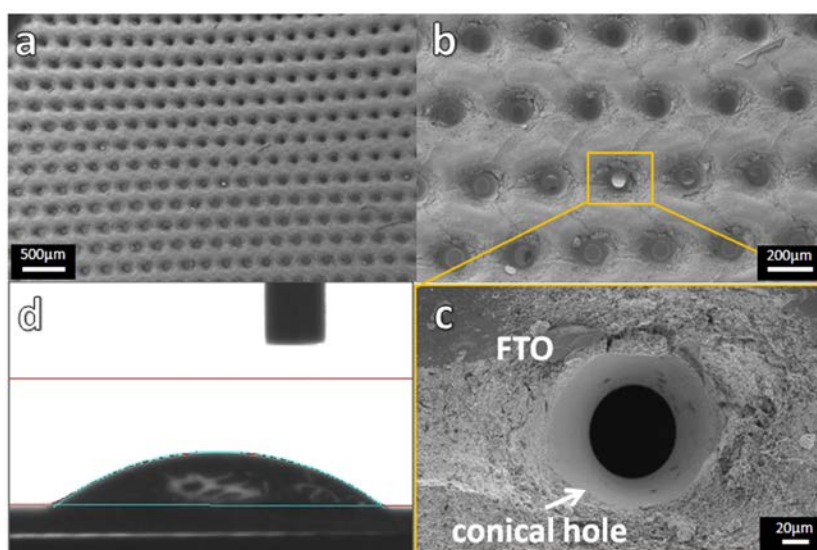


Fig. 5: FESEM images of the laser-drilled electrode: (a,b) top view from FTO side and (c) high magnification of a hole. (d) Optical contact angle on FTO side of the *drilled* electrode.

component) is equal to 14% and this value increases to 37% in the case of *drilled* electrodes, essentially due to the increase of the diffuse component. This is a beneficial effect for applications in water splitting devices, where the light reflected back from the *drilled* electrode surfaces will be easily utilized by the photocatalysts that will be deposited on the electrode surfaces. Additionally, in Fig. 6 also the (1-T-R) spectra is reported, showing that the absorption of *non-drilled* and *drilled* electrodes remains practically unchanged, since the FTO coating in both quartz substrates was made following the same procedure.

The electrical properties of *non-drilled* and *drilled* electrodes have been tested. The measured sheet resistance values of the FTO films were 5 Ω /square for the *non-drilled* and 40 Ω /square for the *drilled* electrodes respectively. This result shows that the drilled FTO surfaces, even with a lower electrical conductivity, still allow good collection of the generated electrons and that the *drilled* electrodes can be conveniently employed within the PEM photo-electrolyzer.

The *drilled* electrodes showed a hydrophilic behavior, well put into evidence through contact angle measurements reported in Fig. 5-d. The good wettability (water contact angle 38.4°) and hydrophilicity of the *drilled* electrodes are key parameters for good adhesion of photocatalyst

materials. In order to prove its applicability, we deposited a titania film on its surface, to then test it in a lab-scale photo-electrolyzer. FESEM images of the resulting *TiO₂/drilled* electrode are shown in Fig. 7-a,b. It is evident the complete and homogeneous coverage of all the surface of the electrode, having star-like openings in the area where the holes are present. The deposited titania film with a thickness of 13.5 μ m (Fig. 7-c,d) is constituted by nanoparticles of about 10-20 nm (see Fig. 7-e). The mean water contact angle value for the *TiO₂/drilled* electrode is equal to 21.3 ° (Fig. 7-f). This good hydrophilicity is also beneficial for a rapid expulsion of the produced gases.

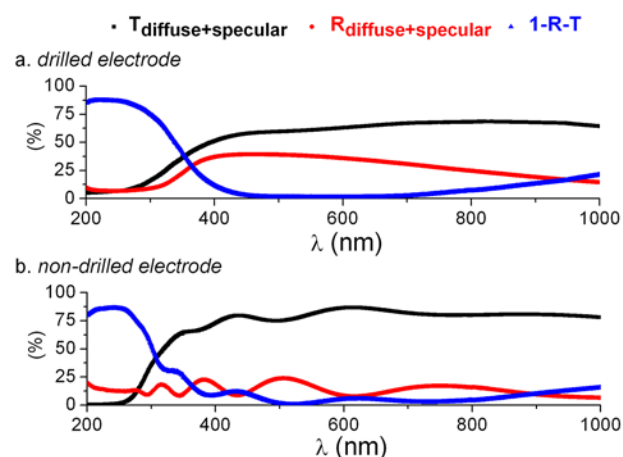


Fig. 6: UV-Vis spectroscopy results of *drilled* (a) and *non-drilled* (b) FTO/quartz electrodes. In the legend, T is the transmittance and R is the reflectance.

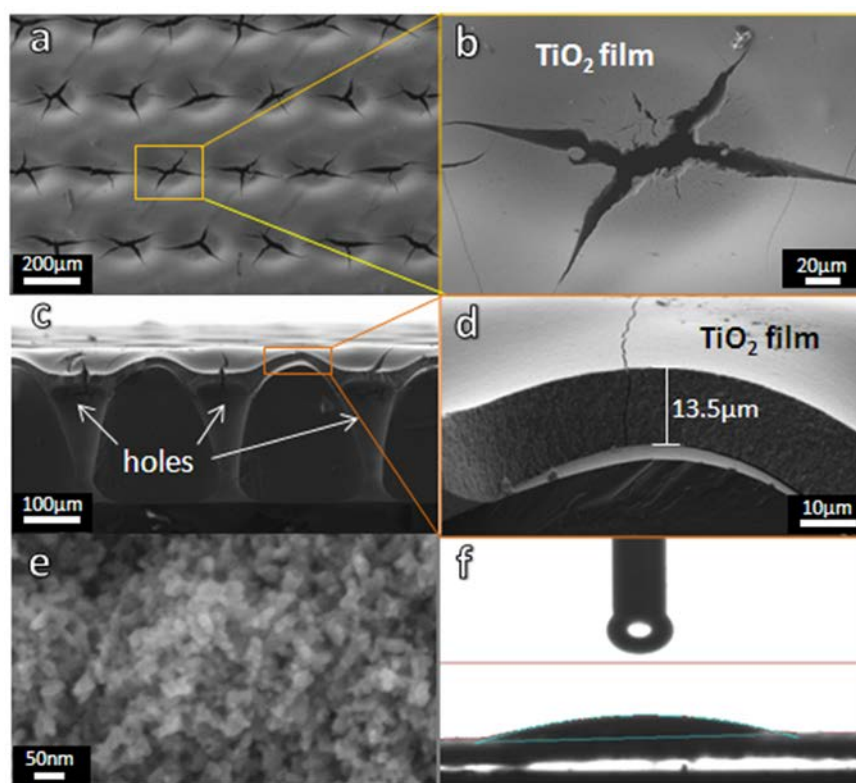


Fig. 7: FESEM images of drilled electrode covered with TiO_2 film: (a,b) top view and magnification of a hole, (c,d) cross section and measurement of titania film thickness, (e) high resolution image of TiO_2 deposited nanoparticles. (f) Optical contact angle of titania in the $\text{TiO}_2/\text{drilled}$ electrode.

A similar behavior is noticed on the *Pt/drilled* electrode, in which the Pt film deposited by sputtering also showed good adhesion and uniform coverage of the drilled FTO surface.

3.2. Electrochemical characterization in Electrolytic Cell

The *I-V* curve obtained from the water electrolysis test of the *drilled* electrode in sodium phosphate buffer is shown in Fig. 8. The cell current is negligible at low voltages and starts to rise at about 1.9 V, that corresponds to the voltage frequently reported in the literature as the “onset potential” for water dissociation [38]. As expected, the onset happens at a higher voltage with respect to the reversible cell potential ($E^\circ_{\text{cell}} = 1.23$ V at 25 °C) for the water splitting reaction. The difference between the E°_{cell} and the onset potential is due to the high activation overvoltage increased by the absence of an anodic catalyst, and the ohmic drop, mainly induced by the liquid electrolyte [11, 12, 39-42]. From Fig. 8, it is also possible to observe a noticeable higher current obtained with the

drilled electrode with respect to the *non-drilled* one. As it will be explained later, this behaviour could be attributed to the higher surface area available for the reaction in the porous *drilled* electrode. In fact, even if this is not the main purpose of the proposed electrode design, drilling conical holes in a substrate and lining them with FTO actually increases the FTO filling factor of the electrodes by a few times, and this is in line with an increase in the current density. Assuming a mean coverage factor of about 0.35 for the FTO deposited on the internal surface of the holes, the surface area of the drilled electrode turns out to be 1.4 times higher than the surface area of the non-drilled ones, consistently with the observed current increase reported in Fig. 8.

Fig. 9 reports the results of EIS measurements performed on the different electrodes. In particular, the Bode plot of the impedance phase of the *drilled* electrode is compared with the *non-drilled* one for different applied bias potentials. Here the charge transfer processes occurring in the cell can be

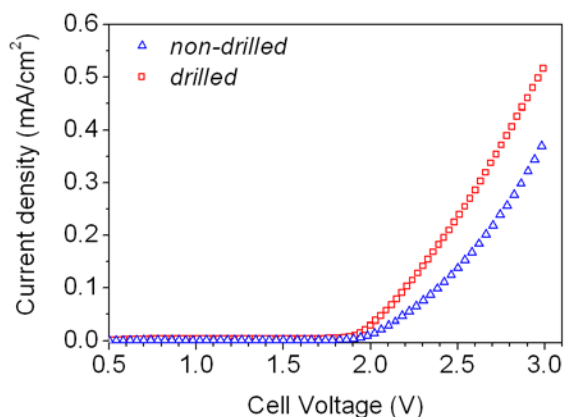


Fig. 8: LSV using the *drilled* and *non-drilled* FTO-covered electrodes as anodes in the electrolytic cell (two-electrodes configuration).

identified thanks to their characteristic peaks, related to their different time constants. The first one at high frequency (HF), in the range between 0.1 and 100 kHz, weakly depends on the applied voltage, and can thus be attributed to the overlap of the electronic transport in the anodic and cathodic electrodes [36]. The second one, at medium-low frequency (LF) in the 0.1 to 100 Hz range, varies with the voltage especially for values higher than the onset potential. Assuming that in our experimental conditions the charge transfer resistance due to the H_2 evolution reaction at the cathodic electrode is negligible with respect to that of the O_2 evolution reaction at the anodic electrode, the dependence of the LF process on the voltage indicates that the process is related to the double layer at the electrolyte/anode interface, that depends on the kinetics of the reaction [36, 43]. For both HF and LF processes, the peaks related to the *drilled* electrodes are always somewhat shifted towards lower frequency with respect to the *non-drilled* one, meaning a slightly slower charge transfer mechanism, as it will be explained below.

All the features discussed above can be also observed in the Nyquist plots of the impedance (Fig. 10). There, each process is related to a semicircle: for voltages lower than the onset one, only a HF semicircle can be clearly distinguishable, while the LF one presents very large curvature radius. While increasing the voltage, also the LF semicircle become visible, due to the higher current density values during the water

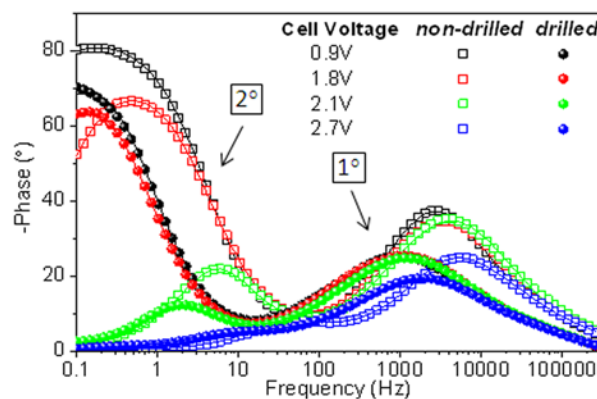


Fig. 9: Bode diagrams of EIS measurements using the *non-drilled* (open symbols) and *drilled* (filled symbols) FTO-covered electrodes as anodes in the electrolytic cell, at different voltages. The lines represent the data fitted by using the equivalent circuit in Fig. 3.

dissociation reaction. It is noteworthy that all the Nyquist plots related to the drilled electrode are characterized by lower impedance values: such result is compatible with the higher current density observed for the *drilled* electrode in the I - V curves.

3.2.1. Fitting of EIS Data

In order to quantitatively evaluate the different parameters of the system and the time constants related to the different processes, a fitting procedure of the experimental impedance data was carried out, using the equivalent circuit depicted in Fig. 3, which has been previously used for modelling EIS data of porous electrodes [3, 10, 36, 37] and for low-current-density PEM-FC [43].

In the proposed circuit, R_s is the series resistance, which includes the FTO film resistance, the resistance of the external electrical contacts, and the resistance of the liquid electrolyte [10, 44]. The HF process at the electrodes is modeled through the parallel $R_{HF} // Q_{HF}$ where Q is a constant phase element (CPE), representing a non-ideal capacitance associated with a normal distribution of time constants through a surface layer, usually employed in systems with distributed porosity or surface roughness [37, 45]. The impedance of a CPE is defined as:

$$Z_{CPE} = \frac{1}{(j\omega)^n Q} \quad (1)$$

where n ($0 < n < 1$) is the CPE index [42, 43]; the

Table 1: EIS fitting results of *non-drilled* and *drilled* electrodes measurements in the electrolytic cell ^a

	Cell Potential (V)	Rs (Ω)	τ _{HF} (s)	C _{HF} (F)	R _{HF} (Ω)	τ _{LF} (s)	C _{LF} (F)	R _{LF} (Ω)	χ ²
<i>non-drilled</i>	0.9	126	1.76E-04	2.20E-07	799	2.30E+01	6.52E-05	353100	4.28E-05
	1.8	131.7	1.48E-04	1.86E-07	797	2.89E+00	5.88E-05	49100	2.50E-04
	2.1	131.9	1.31E-04	1.68E-07	782.5	4.46E-02	3.94E-05	1131	1.84E-04
	2.7	124.3	3.70E-05	1.40E-07	264.5	4.38E-03	3.04E-05	144	1.84E-05
<i>drilled</i>	0.9	98.77	5.21E-04	1.29E-06	403.6	1.00E+01	5.14E-04	19520	1.16E-04
	1.8	99.33	4.02E-04	1.18E-06	340.2	6.74E+00	4.86E-04	13860	5.41E-05
	2.1	100.1	2.94E-04	9.49E-07	309.4	1.05E-01	4.59E-04	228.9	5.04E-05
	2.7	99.65	1.91E-04	8.64E-07	220.7	2.07E-02	2.85E-04	72.67	2.26E-05

^a The electrodes geometric area exposed to the liquid electrolyte is of 4.38 cm²

Table 2: EIS fitting results of *TiO₂/drilled* electrode measurements in the PEM photo-electrolyzer, in the dark and upon simulated solar light illumination (100 mW/cm²) ^b

	Cell Potential (V)	Rs (Ω)	τ _{HF} (s)	C _{HF} (F)	R _{HF} (Ω)	τ _{LF} (s)	C _{LF} (F)	R _{LF} (Ω)	χ ²
dark	0.6	8.03	4.72E-02	8.96E-05	527.1	1.31E+01	7.00E-04	18740	7.89E-04
	1.2	8.04	3.39E-02	6.64E-05	510.1	2.66E+00	5.23E-04	5099	4.14E-04
	1.8	7.59	7.96E-03	3.88E-05	205.2	1.24E-01	3.49E-04	354.6	1.46E-03
	2.4	7.54	3.03E-04	1.99E-05	15.21	1.34E-03	5.12E-05	26.12	1.05E-04
light	0.6	7.27	2.67E-02	5.38E-04	49.67	4.82E+00	9.27E-04	5200	9.52E-05
	1.2	7.32	2.12E-02	4.33E-04	49.06	1.10E+00	7.17E-04	1539	9.97E-05
	1.8	7.71	3.04E-03	2.87E-04	10.62	4.77E-02	3.87E-04	123.3	6.21E-04
	2.4	7.52	1.56E-04	7.46E-05	2.097	1.09E-03	5.13E-05	21.28	2.48E-04

^b The electrodes geometric area exposed to the liquid electrolyte is of 1.59 cm²

capacitance associated with the CPE is given by [46]:

$$C = Q_n^{\frac{1}{n}} R_n^{\frac{1}{n}-1} \quad (2)$$

The elements in the parallel $R_{LF} // Q_{LF}$ represent the charge transfer resistance and the interfacial capacitance associated with the double-layer (LF process). Finally, a Warburg element (Z_w) takes into account the protons diffusion in the electrolyte.

A good agreement between the measured and the fitted data was obtained, as evidenced by the straight curves presented in [Fig.s 9 and 10](#). The superimposition of the curves to the experimental points witnessed that the equivalent circuit is effective for the description of the processes occurring into the system. This feature is successfully confirmed by the Chi-squared parameters reported in [Table 1](#), whose very low values evidence the goodness of the fitting procedure. The parameters calculated through the fitting procedure are reported in [Table 1](#), where the time constant of the i -th process was calculated through the following expression:

$$\tau_i = R_i \cdot C_i \quad (3)$$

To further confirm the fitting goodness, some of the model parameters, namely the ohmic resistances and the time constants, were verified through graphical methods [47], and the obtained values (not reported here) were in good agreement with those extracted from the fitting procedure.

The high R_s values (ranging between 98 and 132 Ω), suggest that the liquid electrolyte gave a great contribution to this parameter, since the values related to FTO layers are one order of magnitude lower. As expected, for low voltages R_{HF} values are quite constant for both electrodes, then become lower above the onset potential. In the meanwhile the anode charge transfer resistances exhibit a large dependance on the applied voltage, compatible with the increase of the electron flow. As already mentioned above, the resistances related to the *drilled* electrodes are lower

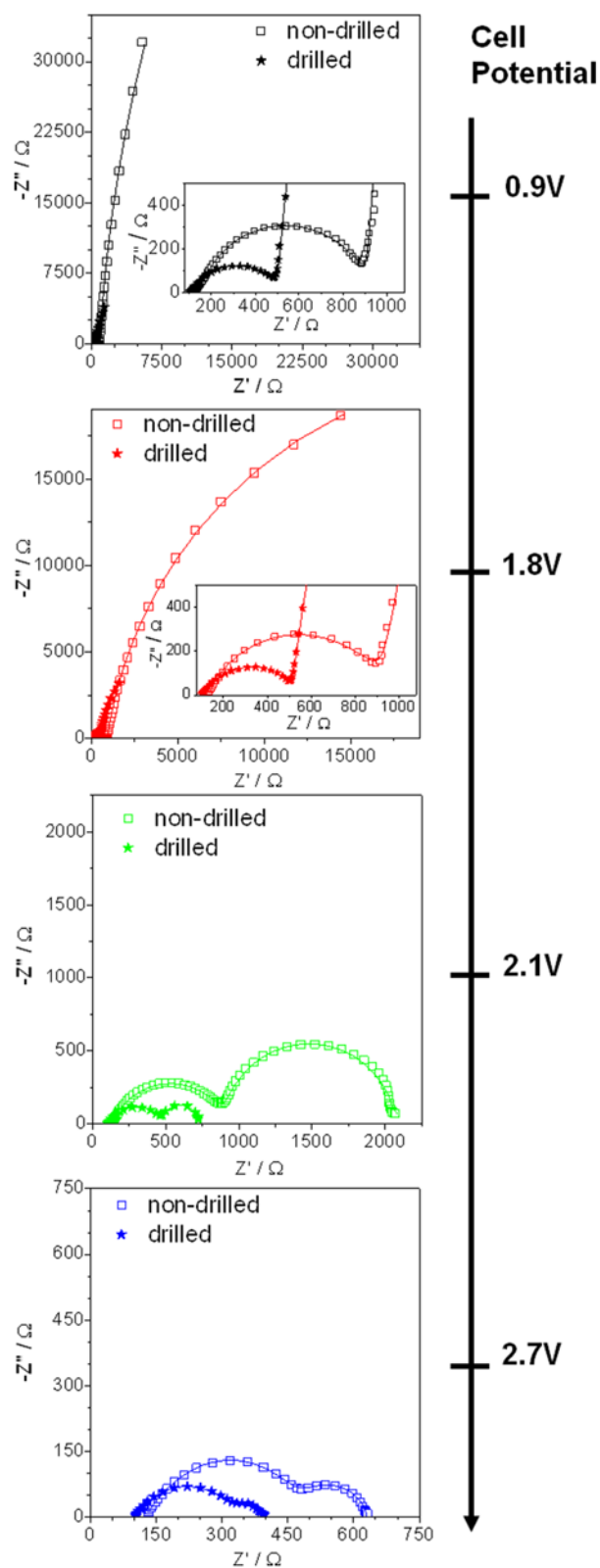


Fig. 10: Nyquist plot from EIS measurements using the *non-drilled* (open symbols) and *drilled* (filled symbols) FTO-covered electrodes as anodes in the electrolytic cell, at different voltages. The lines represent the data fitted by using the equivalent circuit in Fig. 3.

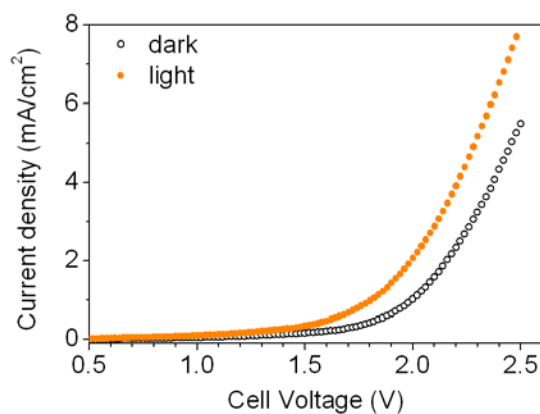


Fig. 11: LSV using the *TiO₂/drilled* electrode as anode in the PEM photo-electrolyzer (two-electrodes configuration).

with respect to the *non-drilled* ones, while the capacitances are one order of magnitude higher, especially those of the double layer. Since the latter is known to be directly proportional to the electrode surface area [48, 49] it follows that, assuming the FTO film in both *drilled* and *non-drilled* electrodes has the same interfacial capacitance per unit area, the obtained capacitance values are a consequence of the higher effective surface area of the *drilled* electrode. Moreover, both time constants values (τ_{HF} and τ_{LF}) are reduced while increasing the applied potential, due to the increase of the current density and the faster kinetics of the anodic reaction, especially above the onset potential. On the other hand, the *drilled* electrode reports slightly higher time constants with respect to the *non-drilled* one, even if they are in the same order of magnitude, indicating the good conductivity of the FTO layer in both substrates. Such results confirm that the reason for the higher current density noticed in the *I-V* curves is the higher exposed surface area in the *drilled* electrode, being the protons pathway equal in both the tests.

Finally, concerning the diffusion in the liquid electrolyte, the fitting values are not reported in Table 1 since these phenomena were only observed for very large potentials in the analyzed frequency range. However, since our aim was the study of the electrode behaviour, we neglected these contributions without losing information on the analysed phenomena in the electrodes.

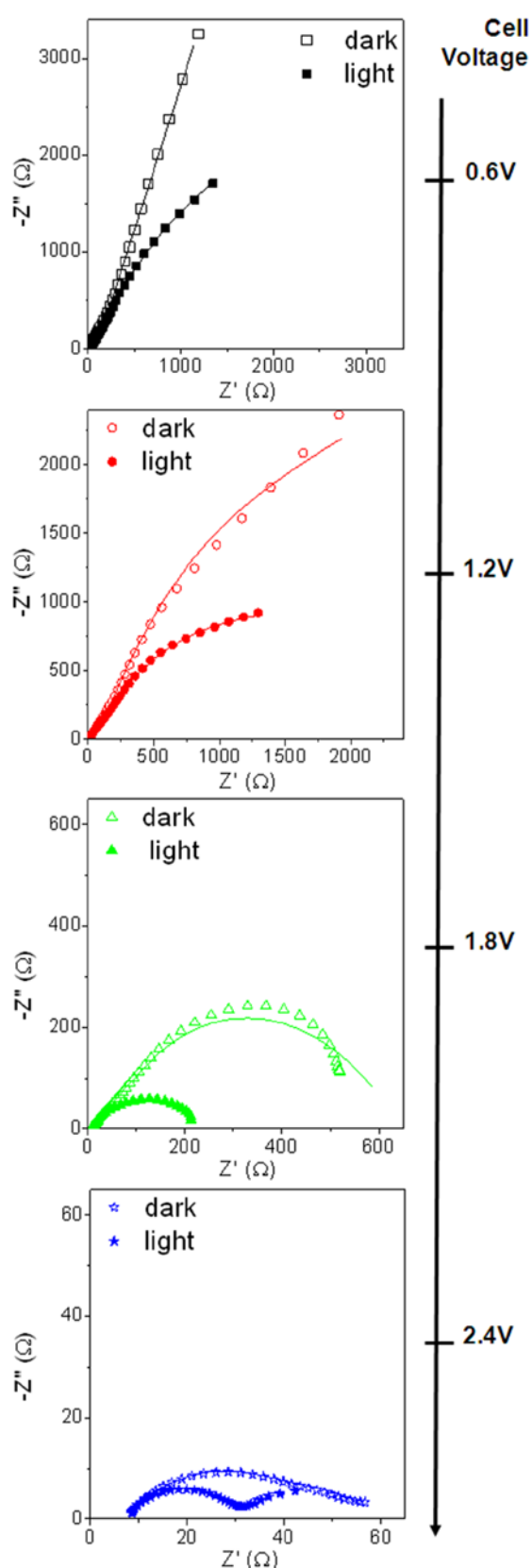


Fig. 12: Nyquist plot from EIS measurements using the *TiO₂/drilled* electrode in the PEM photo-electrolyzer, under dark (open symbols) and under simulated solar light (filled symbols), at different voltages. Lines represent the data fitted by using the equivalent circuit in Fig. 3.

3.3. Photo-electrochemical results in PEM photo-electrolyzer

The *I-V* curve and the EIS results obtained from the water photo-electrolysis tests using the *TiO₂/drilled* electrode in the PEM photo-electrolyzer, in the dark and under simulated solar light, are reported in Figs 11, 12 and 13, respectively. As shown in Fig. 11, the current density obtained in the dark with the PEM device, when operating as an electrolyzer is more than 10-fold higher than the values obtained in the electrolytic cell at 2.4 V vs. RHE. In addition, the onset potential was at about 1.6 V, which is 0.3 V less than in the electrolytic cell, but still at a higher potential with respect to the E°_{cell} for the water splitting reaction. The difference between the E°_{cell} and the onset potential is due to both the activation overvoltages and ohmic potential drop induced by the Nafion membrane, as well as by the interfacial resistance between the polymeric electrolyte and the electrodes [22, 39-42]. Coherently, the impedance values in the PEM photo-electrolyzer (evidenced by the Nyquist diagram in Fig. 12) are one order of magnitude lower with respect to those measured in the electrolytic cell (Fig. 10). Such results are rather good if compared with data reported in the literature for PEM electrolyzers, that usually account for onset potentials between 1.3 and 1.5 V using electrocatalyst based on noble metals such as Ir, coupled with Pt catalysts at the cathode [22-25]. This is the consequence of the use of a more compact structure, like the PEM photo-electrolyzer, which leads to lower ohmic drops than the electrolytic cells, providing a more suitable apparatus for the evaluation of the real performance of catalysts and photo-active materials for water splitting application.

On the other hand, considering that the titania electrode is back-side illuminated, and that the simulated solar light contains about 5% of UV component, the increase of the current under illumination observed in Fig. 11 confirms the good transparency, conductivity and adhesion of the titania in the *TiO₂/drilled* electrode. As expected for a semiconductor photocatalyst, the onset potential shifted to a lower value under illumination (at about

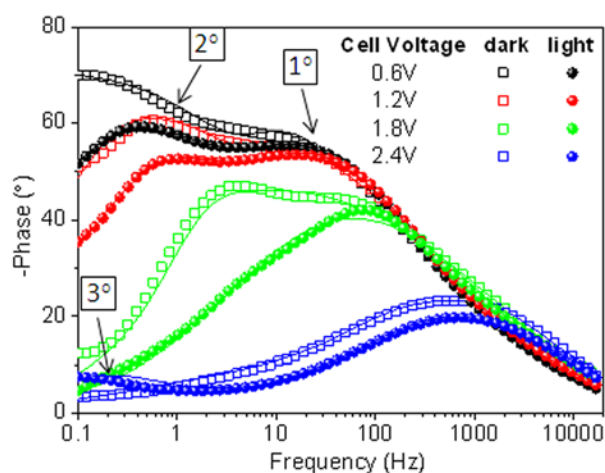


Fig. 13: Bode plots of EIS measurements using the $\text{TiO}_2/\text{drilled}$ electrode in the PEM photo-electrolyzer, under dark (open symbols) and under simulated solar light (filled symbols), at different voltages. The lines represent the data fitted by using the equivalent circuit in Fig. 3.

1.5 V), due to reduction of the internal bias induced by the photo-generation of charge carriers. Under UV illumination, electrons shift from the valence band to the conduction band of the titania and left highly oxidant holes able to perform the water splitting reaction, with a minor activation overpotential with respect to that in dark condition [49]. As a confirmation, from the EIS results shown in Fig. 12, it is evident the reduction of the impedance upon illumination, most remarkable when the onset potential is exceeded.

As for the test in the electrolytic cell, also in this case three different processes can be distinguished, represented by three peaks observed in the Bode diagram on Fig. 13. For low voltages (below the onset potential) two charge transfer processes can be observed: the first one at frequency higher than 10 Hz (HF), that remains constant with the voltage, and the second one below 10 Hz (LF) that shifts towards higher frequency while increasing the applied bias. After the onset potential, the LF charge transfer starts overlapping with the HF one (as seen at 1.8 V), remaining completely superimposed at 2.4 V. In Fig. 13, the effect of the illumination is also visible. In particular, the HF process is not dependent on the illumination, in accordance to the attribution to the charge transfer in the conductive substrates of the

electrodes given above. On the other hand, the LF peaks shifted towards higher frequency upon illumination: in this case this process has to be attributed to the double layer (as in the electrolytic cell) but also to the depletion layer on the titania film, in which the charge transport is enhanced by the band bending under UV illumination [44, 48, 49].

Moreover, in the light-driven measurement taken at high potential (≥ 2.4 V), the presence of a third process is observable in Figs 12 and 13. It is attributed to the diffusion of H^+ ions in the PEM (Nafion 117), that is known to be a slow mass transport process appearing at higher loads and low frequency [42, 43].

Finally, the bubbles formation during the oxygen evolution reaction in the $\text{TiO}_2/\text{drilled}$ electrode, which is expected from the well known catalyst behaviour of TiO_2 , is shown in the inset of Fig. 2-c. This demonstrates that the *drilled* electrode allow a very good adhesion of the catalyst and that the proposed new MEA architecture is an ideal support for testing new anodic and cathodic photoactive materials working in tandem configuration.

3.3.1. Fitting and analysis of EIS Data

EIS results have been simulated using the equivalent circuit represented in Fig 3, and the resulting curves are presented in Figs. 12 and 13, perfectly superimposed on the experimental ones. The parameters obtained from the fitting procedure are reported in Table 2. The series resistance (R_s) in this case was one order of magnitude lower with respect to that obtained in the electrolytic cell, confirming the reduction of the ohmic losses due to both the lower volume of liquid electrolyte in the PEM photo-electrolyzer and the proper conductivity of the Nafion membrane. Moreover, the R_s value of about 8Ω is in agreement with reported values in the literature for semiconductors supported by FTO-covered substrates, validating also the good conductivity of the FTO-*drilled* electrode.

The HF and LF processes were modelled by means of two parallels of resistance and CPE elements: R_{HF}/Q_{HF} and R_{LF}/Q_{LF} , respectively. The HF time constant (τ_{HF}) calculated as in eq. (3), slightly

decreases by increasing the bias potential below the onset voltage, than becomes two orders of magnitude lower for high biases, in accordance to what observed in the Bode plots. On the other hand, the time constant at LF (τ_{LF}) changes obviously with the increase of the applied potential, related with the variation of the double layer at the TiO_2 -electrolyte interface, that in turn mostly depends on the kinetics of the anodic reaction. In addition the effect of illumination on the depletion layer in the semiconductor film is responsible for the higher time constant values observed in dark condition.

From the data reported in [Tables 1 and 2](#), it is important to remark that the double-layer represents the controlling resistance on the photo-electrochemical cell, thus confirming the importance of the development of new photoactive anodic materials, in order to have a breakthrough of the water photolysis technology.

4. CONCLUSIONS

The fabrication and characterization of a transparent electrode with innovative design for application in PEM photo-electrolyzers was presented. Thin quartz sheet covered with FTO were laser-drilled to obtain a transparent and conductive electrode, permeable to water and gases. The transparency of the porous electrode in the visible range was higher than 60% and the electrical sheet resistance was equal to 40 Ω/square : both these parameters are suitable for the application of the electrode in a PEM device for photo-assisted water splitting.

The EIS technique was used as a very powerful tool to gain information on the real active surface of the new *drilled* electrode and on the main electrochemical parameters driving the charge transfer reactions on it. First, the electrode was characterized in an electrolytic cell. A modeling of the EIS curves, with an equivalent electrical circuit, allowed to estimate the governing parameters of the charge transfer processes and put in evidence that the higher exposed surface area of the *drilled* electrode is responsible for the higher observed current density with respect to a *non-drilled* electrode. Subsequently, the drilled electrode

was used as a support for a photocatalytic material (i.e. TiO_2), joined with a Nafion 117 membrane and tested in a compact, miniaturized PEM photo-electrolyzer. Electrochemical characterizations under simulated solar light evidenced the lowering of the onset potential for water splitting reaction and the fastening of the charge transfer processes. These results demonstrate the full applicability of this innovative architecture for the development of new devices with joined anodic/cathodic photocatalysts working in tandem configuration for solar fuel production.

In conclusion, the proposed *drilled* electrode concept and design aims at offering an electrode substrate, well defined from a geometrical viewpoint, for two main purposes: *a)* provide a simple transparent electrode for advanced photo-electrochemical devices [\[7, 8, 50, 51\]](#), *b)* provide an easy-to-model substrate for detailed modeling of the complex multiphase phenomena occurring at the electrodes of an electrolyzer [\[52, 53\]](#).

As for point *a)* it has to be underlined that the manufacturing technique employed for the electrode backbone (laser drilling) on the one hand allows for a precise and reproducible distances among the perforations and conical shape of the holes, but in the other hand cannot be considered at all as a commercially viable technique from either the economical or the environmental footprint (life-cycle assessment) viewpoints. More commercially amenable techniques would have to be exploited in case the proposed concept would demonstrate potential for practical application (e.g. tape casting, use of textiles, mechanical drilling, etc.). Several studies in the leading application field of photo-electrolyzers showed that the transfer of ions between the water splitting anode and the proton recombination cathode may be a performance bottleneck. Particularly, D. Nocera's group showed that this may halve the solar energy to hydrogen conversion efficiency [\[50\]](#). The proposed drilled electrodes offer direct pathways for H^+ transfer from the anode facing sunlight and the rear cathode where hydrogen evolution occurs. Besides, the transparency of the electrode would allow part of the solar spectrum to reach the cathode there possibly

boosting (if suitable dyes are hosted) the proton recombination process.

The number of holes per unit surface we tested may be well in excess to meet these last requirements. The potential for reduction of this parameter, which would bring about a proportional reduction of the electrode manufacturing costs, will be analyzed in future studies of ours.

As for point **b**), the perforated electrode can offer a standardized geometry for in depth studies on the effect of multiphase ion and charge transfer typical of PEM or alkali electrolyzers electrodes. As in the present study, the complex nature of the phenomena occurring at the electrodes is often lumped into a single interface resistance of the electrode [54-56]. Recent modeling and experimental approaches (e.g. by Ito et al. [52, 53]) have analyzed in deeper details the peculiar interphase phenomena occurring at the PEM electrolyzer electrodes, including the effect of capillary forces in multimodal pore size distribution. Particularly, the effect of such phenomena on the electrode interfacial resistance could be approached by these Authors. The availability of equal size pores ordered according to a reproducible and rigorous pattern typical of our laser-drilled electrodes will offer a unique validation platform for such studies.

5. ACKNOWLEDGEMENTS

The authors would like to thank Prof. Paolo Spinelli, Politecnico of Torino, and Prof. Masayuki Itagaki, Tokyo University of Science, for the fruitful discussions and advices. Marco Fontana is thanked for the FESEM measurements. Gustavo Guajardo and Alessandro Nesca are acknowledged for the technical support in the design and fabrication of the PEM photo-electrolyzer housing. The financial support from the European Commission on the 7th Framework Program (NMP-2012 Project Eco²CO₂ nr.309701 and FCH-JU Call 2011-1 Project ArtipHycion nr.303435) is gratefully acknowledged.

6. REFERENCES

- [1] A. Fujishima, K. Honda, *Nature*, 238 (1972) 37-38.
- [2] K. Sivula, F. Le Formal, M. Grätzel, *ChemSusChem*, 4 (2011) 417-417.
- [3] A. Tacca, L. Meda, G. Marra, A. Savoini, S. Caramori, V. Cristino, C.A. Bignozzi, V. Gonzalez Pedro, P.P. Boix, S. Gimenez, J. Bisquert, *ChemPhysChem*, 13 (2012) 3025-3034.
- [4] H. Wu, Z. Zhang, *International Journal of Hydrogen Energy*, 36 (2011) 13481-13487.
- [5] Z. Yi, J. Ye, N. Kikugawa, T. Kako, S. Ouyang, H. Stuart-Williams, H. Yang, J. Cao, W. Luo, Z. Li, Y. Liu, R.L. Withers, *Nat Mater*, 9 (2010) 559-564.
- [6] S. Zanarini, S. Vankova, S. Hernandez, V.S. Ijeri, M. Armandi, E. Garrone, B. Bonelli, B. Onida, P. Spinelli, *Chemical Communications*, 48 (2012) 5754-5756.
- [7] S. Bensaid, G. Centi, E. Garrone, S. Perathoner, G. Saracco, *ChemSusChem*, 5 (2012) 500-521.
- [8] D.G. Nocera, *Accounts of Chemical Research*, 45 (2012) 767-776.
- [9] A.J. Bard, M.A. Fox, *Accounts of Chemical Research*, 28 (1995) 141-145.
- [10] T. Lopes, L. Andrade, H.A. Ribeiro, A. Mendes, *International Journal of Hydrogen Energy*, 35 (2010) 11601-11608.
- [11] J.O.M.S.S. Bockris, *Fuel cells: their electrochemistry*, in, McGraw-Hill, New York, 1969.
- [12] T. Thampam, S. Malhotra, J. Zhang, R. Datta, *Catalysis Today*, 67 (2001) 15-32.
- [13] F. Barbir, *Solar Energy*, 78 (2005) 661-669.
- [14] S.A. Grigoriev, V.I. Porembsky, V.N. Fateev, *International Journal of Hydrogen Energy*, 31 (2006) 171-175.
- [15] Project SOLHYDROMICS: Nanodesigned electrochemical converter of solar energy into hydrogen hosting natural enzymes or their mimics, in, 7th Framework Programme FET call 2009, nr. 227192.
- [16] Project ArtipHycion: Fully artificial photo-electrochemical device for low temperature hydrogen production, in, 7th Framework Programme FCH-JU Call 2011-1, nr.303435.
- [17] Project: Eco-friendly biorefinery fine chemicals from CO₂ photo-catalytic reduction, in, 7th Framework Programme NMP-2012, nr.309701.
- [18] B. Klahr, S. Gimenez, F. Fabregat-Santiago, T. Hamann, J. Bisquert, *Journal of the American Chemical Society*, 134 (2012) 4294-4302.
- [19] C. Fàbrega, T. Andreu, A. Tarancón, C. Flox, A. Morata, L. Calvo-Barrio, J.R. Morante, *International Journal of Hydrogen Energy*, 38 (2013) 2979-2985.
- [20] R. Brimblecombe, A. Koo, G.C. Dismukes, G.F. Swiegers, L. Spiccia, *Journal of the American Chemical*

Society, 132 (2010) 2892-2894.

[21] F. Marangio, M. Santarelli, M. Calì, *International Journal of Hydrogen Energy*, 34 (2009) 1143-1158.

[22] M. Carmo, D.L. Fritz, J. Mergel, D. Stolten, *International Journal of Hydrogen Energy*, 38 (2013) 4901-4934.

[23] S.J. Peighambaroust, S. Rowshanzamir, M. Amjadi, *International Journal of Hydrogen Energy*, 35 (2010) 9349-9384.

[24] P. Millet, R. Ngameni, S.A. Grigoriev, N. Mbemba, F. Brisset, A. Ranjbari, C. Etievant, *International Journal of Hydrogen Energy*, 35 (2010) 5043-5052.

[25] S.-D. Yim, G.-G. Park, Y.-J. Sohn, W.-Y. Lee, Y.-G. Yoon, T.-H. Yang, S. Um, S.-P. Yu, C.-S. Kim, *International Journal of Hydrogen Energy*, 30 (2005) 1345-1350.

[26] O. Winther-Jensen, K. Chatjaroenporn, B. Winther-Jensen, D.R. MacFarlane, *International Journal of Hydrogen Energy*, 37 (2012) 8185-8189.

[27] K.-T. Jeng, Y.-C. Liu, Y.-F. Leu, Y.-Z. Zeng, J.-C. Chung, T.-Y. Wei, *International Journal of Hydrogen Energy*, 35 (2010) 10890-10897.

[28] A. Kargar, K. Sun, Y. Jing, C. Choi, H. Jeong, G.Y. Jung, S. Jin, D. Wang, *ACS Nano*, 7 (2013) 9407-9415.

[29] E. Arsenault, N. Soheilnia, G.A. Ozin, *ACS Nano*, 5 (2011) 2984-2988.

[30] P.G. Hoertz, Z. Chen, C.A. Kent, T.J. Meyer, *Inorganic Chemistry*, 49 (2010) 8179-8181.

[31] S. Chen, S.-Z. Qiao, *ACS Nano*, (2013) DOI: 10.1021/nn404444r.

[32] J. Wang, S. Pan, M. Chen, D.A. Dixon, *The Journal of Physical Chemistry C*, 117 (2013) 22060-22068.

[33] L. Wang, C.-Y. Lee, P. Schmuki, *Electrochimica Acta*, 91 (2013) 307-313.

[34] H. van't Spijker, D. Simon, F. Ooms, *International Journal of Hydrogen Energy*, 33 (2008) 6414-6419.

[35] D.K. Owens, R.C. Wendt, *Journal of Applied Polymer Science*, 13 (1969) 1741-1747.

[36] C. Hitz, A. Lasia, *Journal of Electroanalytical Chemistry*, 500 (2001) 213-222.

[37] X. Dominguez-Benetton, S. Sevda, K. Vanbroekhoven, D. Pant, *Chemical Society Reviews*, 41 (2012) 7228-7246.

[38] C.C. Hu, Y. Wu, *Materials Chemistry and Physics*, 82 (2003) 588-596.

[39] L. You, H. Liu, *Journal of Power Sources*, 155 (2006)

219-230.

[40] P. Choi, D.G. Bessarabov, R. Datta, *Solid State Ionics*, 175 (2004) 535-539.

[41] D.M. Bernardi, M.W. Verbrugge, *Journal of The Electrochemical Society*, 139 (1992) 2477-2491.

[42] M.E. Orazem, B. Tribollet, *Time-Constant Dispersion*, in: *Electrochemical Impedance Spectroscopy*, John Wiley & Sons, Inc., 2008, pp. 233-263.

[43] E. Barsoukov, J.R. Macdonald, *Impedance Spectroscopy: Theory, Experiment, and Applications*, Wiley, 2005.

[44] N. Baram, Y. Ein-Eli, *The Journal of Physical Chemistry C*, 114 (2010) 9781-9790.

[45] J. Bisquert, G. Garcia-Belmonte, F. Fabregat-Santiago, N.S. Ferriols, P. Bogdanoff, E.C. Pereira, *The Journal of Physical Chemistry B*, 104 (2000) 2287-2298.

[46] B. Hirschorn, M.E. Orazem, B. Tribollet, V. Vivier, I. Frateur, M. Musiani, *Electrochimica Acta*, 55 (2010) 6218-6227.

[47] M.E. Orazem, B. Tribollet, *Preliminary Graphical Methods*, in: *Electrochemical Impedance Spectroscopy*, John Wiley & Sons, Inc., 2008, pp. 333-351.

[48] L.M. Peter, D.J. Riley, R.I. Wielgosz, *Applied Physics Letters*, 66 (1995) 2355-2357.

[49] J.J. Kelly, Z. Hens, D. Vanmaekelbergh, Z. Hensalzo, *Photoelectrochemical Systems Characterization*, in: *Encyclopedia of Electrochemistry*, Wiley-VCH Verlag GmbH & Co. KGaA, 2007.

[50] S.Y. Reece, J.A. Hamel, K. Sung, T.D. Jarvi, A.J. Esswein, J.J.H. Pijpers, D.G. Nocera, *Science*, 334 (2011) 645-648.

[51] D. Gust, T.A. Moore, A.L. Moore, *Accounts of Chemical Research*, 42 (2009) 1890-1898.

[52] H. Ito, T. Maeda, A. Nakano, C.M. Hwang, M. Ishida, A. Kato, T. Yoshida, *International Journal of Hydrogen Energy*, 37 (2012) 7418-7428.

[53] H. Ito, T. Maeda, A. Nakano, A. Kato, T. Yoshida, *Electrochimica Acta*, 100 (2013) 242-248.

[54] S. Sawada, T. Yamaki, T. Maeno, M. Asano, A. Suzuki, T. Terai, Y. Maekawa, *Progress in Nuclear Energy*, 50 (2008) 443-448.

[55] A. Ursúa, P. Sanchis, *International Journal of Hydrogen Energy*, 37 (2012) 18598-18614.

[56] M. Shen, N. Bennett, Y. Ding, K. Scott, *International Journal of Hydrogen Energy*, 36 (2011) 14335-14341.